Table of Contents

List of Figures

Chapter 1

Glossary

EL Entrainment Layer

ML Mixed Layer

CBL Convective Boundary Layer

LES Large Eddy Simulation

FA Free Atmosphere

GCM General Circulation Model

DNS Direct Numerical Simulation

TKE Turbulence Kinetic Energy

Ri Richardson Number, the bulk Richardson Number is $\frac{gh}{\overline{\theta}_{ML}}\frac{\Delta\theta}{w^{*2}}$, $\Delta\theta = \overline{\theta}(h_1) - \overline{\theta}(h_0)$

Chapter 2

Introduction

2.1 Motivation and Research Questions

The daytime convective atmospheric boundary layer (CBL) over land starts to grow at sunrise when the surface becomes warmer than the air above it. Coherent turbulent structures (thermals) begin to form and rise since their relative warmth causes them to be less dense and so buoyant. The temperature profile of the residual nightime boundary layer is stable i.e. potential temperature (θ) increases with height. The thermals rise to their neutral bouoyancy level overshoot and then overturn or recoil concurrently dragging down warm stable air from above which is subsequently mixed into the growing turbulent mixed layer (ML) (Stull 1988). This mixing at the top of the CBL is known as entrainment and the region over which it occurs, the entrainment layer (EL). CBL entrainment occurrs via distortion of buoyancy driven thermals by the buoyancy difference (θ jump) caused upon overshoot. These opposing buoyant forcings make for interesting dynamics.

CBL height (h) and the prediction thereof are important for calculating the concentration of any species as well as the sizes of the turbulent structures. In combination with the lifting condensation level knowledge of EL depth allows predictions pertaining to the formation of cumulous clouds. For example cloud cover increases as more thermals rise above their lifting condensation level. Parametrizations for both CBL growth and EL depth are required in mesoscale and general circulation models (GCMs). Furthermore it is an attractive goal to develop a robust set of scales for this region analogous to Monin-Obvukov Theory (Stull 1988, Traumner et al. 2011, Steyn et al. 1999, Nelson et al. 1989, Sorbjan 1996)

An effective, simplified conceptual model of the dry, shear-free CBL in the absence of large scale winds is represented in Figure 2.1. Turbulent mixing via upward moving thermals and corresponding cooler dowdraughts renders the average potential temperature $\overline{\theta}$ effectively constant within the ML. The average vertical turbulent heat flux ($\overline{w'\theta'}$) is positive and decreases as the thermals approach the CBL top. In the EL there is a mixture of turbulent thermals and relatively warmer stable air. The proportion of the latter increasing with proximity to the free atmosphere (FA) above. In the EL $\overline{w'\theta'}$ becomes negative as the thermals, which are now relatively cool, impinge on the FA and turn downward pulling warmer air with them. The dimensionless parameter that represents the forcings under these conditions, and is ubiquitous in the corresponding literature, is the convective or buoyancy Richardson number: Ri $= \frac{\frac{g}{\overline{\theta}_{ML}}\Delta\theta h}{w^{*2}}$ (Deardorff et al. 1980, Stull 1988, Sullivan et al. 1998, Federovich et al. 2004, Brooks and Fowler 2012, Garcia and Mellado 2014). h is the CBL height and w^* is the convective velocity scale (Deardorff 1970) to be defined later.

The two principal external parameters in this simplified case, i.e. the dry, shear-free CBL in the absence of large scale winds, are the average vertical turbulent surace heat flux ($\overline{w'\theta'}_s$) and the upper lapse rate (γ) (Federovich et al. 2004,Sorbjan 1996). They have opposing effects, that is $\overline{w'\theta'}_s$ drives upward turbulent velocity (${w'}^+$) and so CBL growth (w_e) wheras γ suppresses it. Conversely they both cause positive turbulent potential temperature perturbations (${\theta'}^+$) and so warming of the CBL. In the EL the thermals from the surface are now relatively cool. They turn downwards as they interact with the stable FA concurrently bringing down warmer sta-

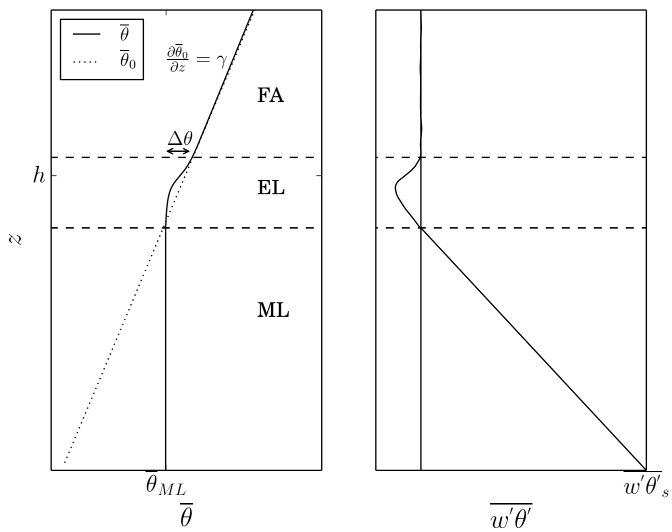

Figure 2.1: The ML, EL and FA as represented by idealized vertical $\overline{\theta}$ and $\overline{w'\theta'}$ profiles.$\overline{\theta}_0$ is the initial $\overline{\theta}$.

ble are from above. Sullivan et al. (1998) demonstrated these dynamics by partitioning $w^{'}\theta^{'}$ into four quadrants: upward moving warm ($w^{'+}\theta^{'+}$), downward moving warm ($w^{'-}\theta^{'+}$), upward moving cool ($w^{'+}\theta^{'-}$) and downward moving cool ($w^{'-}\theta^{'-}$). Sorbjan 1996 asserted and showed that in this region the potential temperature perturbations ($\theta^{'}$) are strongly influenced by γ whereas the turbulent vertical velocity peturbations ($w^{'}$) are almost independent thereof. Inspired by these two studies and to gain some insight into the dynamics of this idealized CBL I ask **Q1: How does the distrubutions of local CBL height, and the joint distrubutions of $w^{'}$ and $\theta^{'}$ within the EL, vary with $\overline{w'\theta'}_s$ and γ?**

The relationship between scaled EL depth and Ri

$$\frac{\Delta h}{h} \propto Ri^b \tag{2.1}$$

has been explored and justified in field measurement, laboratory, numerical studies. There is disagreement with respect to its exact form, in part stemming from variation in height and θ jump defininitions, but general its magnitude relative to h decreases with increasing Ri. Although referred to in most relevant studies to and relied upon in analytical models, the average potential temperature profile has not been used to define the EL (Deardorff et al. 1980, Nelson et al. 1989, Federovich et al. 2004, Boers 1989, Brooks and Fowler 2012). This leads me to ask **Q2: Can the EL limits be defined based on the $\overline{\theta}$ profile and what is the relationship of the resulting depth (Δh) to Ri?**

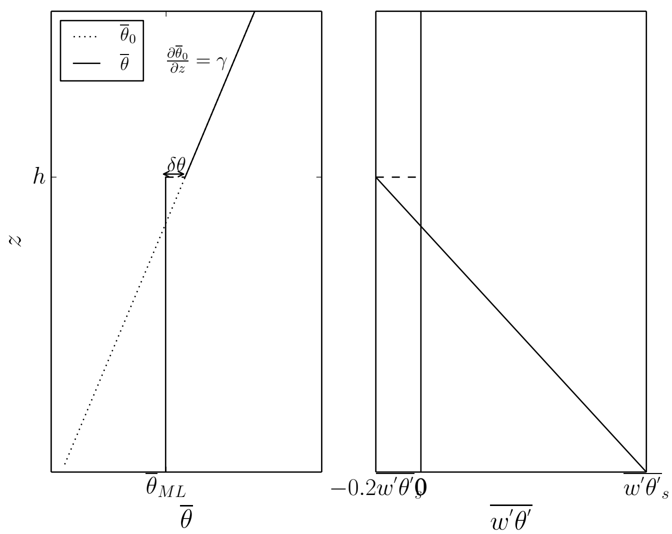

Figure 2.2: A further simplified version of Figure 2.1. The EL is infinitessimely thin.

A further simplification to the dry, shear-free, CBL model without large scale velocities, is to regard the EL depth as infinitessimly small as in Figure 2.2. The relationship of the scaled, time rate of change of h (entrainment rate: w_e) to Ri can be derived based on this model (Tennekes 1973, Deardorff 1979, Federovich et al. 2004)

$$\frac{w_e}{w^*} \propto Ri^a \tag{2.2}$$

.

This will be referred to as the entrainment relation. Although that there is such a relationship is well esablished, discussion as to the power exponent of Ri is unresolved and results from studies justify values of both $-\frac{3}{2}$ and -1. See Traumner et al. (2011) for a summary and review. Turner (1986) explains this disparity in terms of entrainment mechanism such that the higher value occurrs when thermals recoil rather than overturn in response to a stronger θ jump (or inversion). Whereas Sullivan et al. (1998) notice a deviation from the lower power (-1) at lower Ri and attribute it to the effect of a the shape of $\overline{\theta}$ within a thicker EL. Both Federovich et al. (2004) and Garcia and Mellado (2014) show how the definition of the θ jump influences the time rate of change of Ri and so effects a. **Q3: How does defining the θ jump based on the vertical $\overline{\theta}$ accross the EL as in Figure 2.1 vs at the inversion (h) as in Figure 2.2, effect the entrainment relation and in particular a?**

2.2 Relevant Background

2.2.1 The Convective Boundary Layer (CBL)

The CBL starts to grow rapidly at sunrise, peaking at midday. Convective turbulence and the dominant upward vertical motions then begin to subside as the surface cools. While the surface is warm, buoyancy driven thermals of uniform potential temperature (θ) and tracer concentration at their cores form and entrain surrounding air laterally as they rise, as well as trapping and mixing in stable warm from above (Stull 1988, Crum et al. 1987). Under conditions of strong convection, buoyantly driven turbulence dominates and shear is insignificant (Fedorovich and Conzemius 2001). Thermal overshoot relative to their neutral buoyancy level, and subsequent entrainment of the warmer air from aloft augments the warming caused by the surface heat flux ($\overline{w'\theta'}_s$) and results in a potential temperature jump ($\Delta\theta$) or inversion at the CBL top (Schmidt and Schumann 1989, Turner 1986). There may also be a residual inversion from the day before possibly strengthened by subsidence, i.e. large scale downward movenent of warmer air from above (Stull 1988, Sullivan et al. 1998).

Lidar images show the overall structure of the CBL with rising thermals, impinging on the air above (Crum et al. 1987, Traumner et al. 2011). This has been effectively modelled using large eddy simulation (LES) by Schmidt and Schumann (1989) who used horizontal slices of potential temperature and vertical velocity perturbations ($\theta^{'}$, $w^{'}$) at various vertical levels to show how the thermals form, merge and impinge at the CBL top with concurrent peripheral downward motions. The latter is supported in the visualizations of Sullivan et al. (1998). Vertical cross sections within the EL show the relatively cooler thermals and trapped warmer air as well as the closely associated upward motion of cooler air and downward motion of warmer air.

On average these convective turbulent structures create a fully turbulent mixed layer (ML) with eddie sizes cascading through an inertial subrange to the molecular scales at which energy is lost via viscous dissipation (Stull 1988). Here $\overline{\theta}$ is close to uniform and increases with respect to time due to $\overline{w'\theta'}_s$ and the flux of entrained stable air at the inversion ($\overline{w'\theta'}_h$). ML turbulence is dominated by warm updraughts and cool downdraughts. With proximity to the top the updraughts become relatively cool and warmer air from above is drawn downward, so in the ML $\overline{w'\theta'}$ is positive and decreasing. Above the ML the air becomes more stable with altitude and, on average, transitions from a uniform ML potential temperature ($\frac{\partial\overline{\theta}}{\partial z} \approx 0$) to a stable lapse rate (γ). A peak in the average vertical gradient ($\frac{\partial\overline{\theta}}{\partial z}$) at the inversion represents regions where thermals have exceeded their neutral buoyancy level.

Nelson et al. (1989) outline the stages of CBL growth from when the sublayers of the nocturnal boundary layer are entrained, until the previous day's capping inversion is reached and a quasi-steady growth is attained. The EL depth relative to CBL height varies throughout these stages and its relationship to scaled entrainment is hysteresial. Numerical studies typically represent this last quasi-steady phase involving a constant $\overline{w'\theta'}_s$ working against an inversion and or a stable γ (Schmidt and Schumann [16], Sorbjan 1996, Sullivan et al. 1998, Federovich et al. 2004, Brooks and Fowler 2012).

2.2.2 Convective Boundary Layer Height (h)

The ML is fully turbulent with an on uniform average potential temperature ($\overline{\theta}$). Aerosol and water vapour concentrations decrease dramatically with transition to the stable upper free atmosphere (FA). So any of these characteristics can support a definition of CBL height (h). Nelson et al. (1989) defined h in terms of the percentage of ML air and identified it by eye from Lidar back-scatter images. Traumner et al. (2011) compared four automated methods applied to Lidar images: a suitable threshold value above which the air is categorized as ML air, the point of minimum (largest negative) vertical gradient, the point of minimum vertical gradient based on a fitted idealized curve, and the maximum wavelet covariance. CBL height detection is a wide and varied field. Both Brooks and Fowler (2012) and Traumner et al. 2011 provide more thorough reviews.

Numerical models produce hundreds of local horizontal points from which smooth averaged vertical profiles be obtained, and statistically robust relationships inferred. Brooks and Fowler (2012) applied a wavelet technique to identify the point of maximum covariance in a local vertical tracer profiles in their large eddy simulation (LES) study. They compared this method to the gradient method i.e. locating the point of maximum vertical gradient, as well as the point of minimum $\overline{w'\theta'}$. This last definition is common among LES and laboratory studies where it has been referred to as the inversion height (Deardorff et al. 1980, Sorbjan 1999, Federovich et al. 2004). Sullivan et al. (1998) clarified that the extrema of the four $\overline{w'\theta'}$ quadrants ($\overline{w'^+\theta'^+}$), $\overline{w'^-\theta'^+}$, $\overline{w'^+\theta'^-}$, $\overline{w'^-\theta'^-}$) in the EL more or less correspond to the average point of maximum $\frac{\partial\overline{\theta}}{\partial z}$, whereas the point of minimum $\overline{w'\theta'}$ was consistently lower. They defined CBL height based on local $\frac{\partial\theta}{\partial z}$ and applied horizontal averaging as well as two methods based on $\overline{w'\theta'}$ for comparison.

So far, no published LES study so far defines the height in terms of the $\overline{\theta}$ or $\frac{\partial\overline{\theta}}{\partial z}$ profile even though analyitical models, from which CBL growth parametrizations stem, rely on an idealized version thereof. Garcia and Mellado 2014 do include it as one of their measures of CBL height in their direct numerical simulation (DNS) study.

2.2.3 Convective Boundary Layer Growth by Entrainment

The CBL grows by trapping pockets of warm stable air between or adjacent to impinging thermal plumes. Traumner et al. (2011) summarize two categories of CBL entrainment:

- Non turbulent fluid can be engulfed between or in the overturning of thermal plumes. This kind of event has been supported by the visualizations in Sullivan et al.'s (1998) LES study as well as in Traumner et al.'s (2011) observations. In both it appeared to occur under a weak inversion or upper lapse rate (γ)

- Impinging thermal plumes distort the inversion interface dragging wisps of warm stable air down at their edges or during recoil under a strong inversion or lapse rate. This type of event is supported by the findings of both Sullivan et al. (1998) and Traumner et al. (2011).

Shear induced instabilities do occur at the top of the atmospheric boundary layer and in some laboratory studies of turbulent boundary layers, under conditions of very high stability, the breaking of internal waves have been observed. Entrainment via, the former is relatively insignificant in strong convection, and the latter has not been directly observed in real or modeled atmospheric CBLs over the range of Ris considered here (Traumner et al. 2011, Sullivan et al. 1998).

2.2.4 The Convective Boundary Layer Entrainment Layer

The ML is fully turbulent but the top is characterised by stable air with intermittent turbulence due to the higher reaching thermals. Garcia and Mellado (2014) demonstrate that the EL is subdivided in terms of length and buoyancy scales. That is, the lower region is comprised of mostly turbulent air with pockets of stable warmer air that are quickly mixed, and so scales with the convective scales (see section 2.4). Whereas the upper region is mostly stable apart from the impinging thermals so scaling here is more influenced by the lapse rate (γ). In the EL the average vertical heat flux ($\overline{w'\theta'}$) switches sign relative to that in the ML. The fast updraughts are now relatively cool ($w'^{+}\theta'^{-}$). In their analysis of the four $\overline{w'\theta'}$ quadrants Sullivan et al. ([23]) concluded that the overall net dynamic in this region is downward motion of warm air from the free atmosphere (FA) ($\overline{w'^{-}\theta'^{+}}$) since the other three quadrants effectively cancel.

In terms of tracer concentration and for example based on a Lidar backscatter profile, there are two ways to conceptually define the entrainment layer (EL). It can be thought of as the range in space (or time) over which local CBL height varies (Crum et al. 1987) or a local region over which the concentration (or back-scatter intensity) transitions from ML to free atmospheric (FA) values (Traumner et al. 2011). The latter can be estimated using either curve-fitting and wavelet techniques (Traumner et al. [25], Steyn et al. [19], Brooks and Fowler [4]).

Although Brooks and Fowler apply a wavelet technique to tracer profiles for the determination of EL limits, in their LES study ([4]) it is more common in numerical modelling and laboratory studies for the EL limits to be defined based on the average vertical turbulent heat flux ($\overline{w'\theta'}$) i.e. the point at which it goes from positive to negative values, and the point at which it goes from a negative value to zero as shown in Figure 2.1 (Deardorff et al. 1980, Federovich et al. 2004, Garcia and Mellado 2014). Analytical models based on the representation in Figure 2.1 assume the region of negative $\overline{w'\theta'}$

coincides with the region where $\overline{\theta}$ transitions from the ML value to the FA value. (Deardorff 1979, Federovich et al. 2004) but no modelling studies use the vertical $\overline{\theta}$ profile to define the (EL).

Since $\overline{\theta}$ modeled by an LES is not strictly constant with respect to height in the ML (Federovich et al. 2004), a threshold value for $\overline{\theta}$ or its vertical gradient must be chosen to identify the lower EL limit. In their 2012 LES study Brooks and Fowler encountered inconsistencies when determining the EL limits from the average tracer profile. Although their tracer profile was quite different to a simulated CBL $\overline{\theta}$ profile, this could serve as cautionary note.

Our understanding of the the characterstics and dynamics of the atmospheric CBL entrainment layer (EL) evolves with the increasing body of measurement (Traumner et al. 2011, Nelson et al. 1989), laboratory (Deardorff et al. 1980) and numerical studies (Deardorff 1972, Sorbjan 1996, Sullivan et al. 1998, Federovich et al. 2004, Brooks and Fowler 2012, Garcia and Mellado 2014). Parametrizations are derived based on analytical models and are validated using LES output and measurements (Federovich et al. 2004, Boers 1989). So the relationship between theory, numerical simulation and measurement is inextricable and any study based on one must refer to at least one of the others.

2.3 Modelling the Convective Boundary Layer and Entrainment Layer

2.3.1 Bulk Analytical Models

Bulk analytical models for the Convective Boundary layer (CBL) derived based on average, vertical profiles of ML quantities can be subdivided into: (i) zero order as represented in Figure 2.2 and (ii) first (and higher) order bulk models as represented in Figure 2.1. The order refers to the shape of the assumed EL.

Zero order bulk models assume a mixed layer (ML) of uniform potential temperature ($\overline{\theta}_{ML}$) topped by an infinitesimally thin layer across which there is a temperature jump ($\delta\theta$) and above which is a constant lapse rate (γ). The assumed average vertical turbulent heat flux ($\overline{w'\theta'}$) decreases linearly from the surface up, reaching a maximum negative value ($\overline{w'\theta'}_h$) which is a constant proportion of the surface value (usually $-.2\overline{w'\theta'}_h$) at the temperature inversion, and decreasing to zero accross the jump. Equations for the evolution of CBL height, $\overline{\theta}_{ML}$ and $\Delta\theta$ are derived on this basis (Tennekes 1973).

If the CBL height (h) is rising, air is being drawn in from the stable layer above and cooled i.e. it is decreasing in enthalpy. The rate of decrease in enthalpy with respect to time is $c_p\rho\Delta\theta\frac{dh}{dt}$ per unit of horizontal area. Since the lapse rate above the inversion is stable Tennekes (1973) equates this enthalpy loss to the average vertical turbulent heat flux at the inversion

$$\Delta\theta\frac{dh}{dt} = -\overline{w'\theta'}_h \tag{2.3}$$

.

The ML warming rate is arrived at via the simplified Reynolds averaged conservation of enthalpy, for which the full derivation is shown in an appendix

$$\frac{\partial\overline{\theta}_{ML}}{\partial t} = -\frac{\partial}{\partial z}\overline{w'\theta'} \tag{2.4}$$

.

Assuming $\overline{w'\theta'}$ has a constant slope this becomes

$$\frac{\partial\overline{\theta}_{ML}}{\partial t} = \frac{\overline{w'\theta'}_s - \overline{w'\theta'}_h}{h} \tag{2.5}$$

,

and the evolution of the temperature jump ($\delta\theta$) depends on the rate of CBL height (h) increase, the upper lapse rate γ and the ML warming rate

$$\frac{d\delta\theta}{dt} = \gamma\frac{dh}{dt} - \frac{d\overline{\theta}_{ML}}{dt} \tag{2.6}$$

.

An assumption about the vertical heat flux at the inversion (h), such as the entrainment ratio, closes this set

$$\frac{\overline{w'\theta'}_h}{\overline{w'\theta'}_s} = -.2 \tag{2.7}$$

.

The relevant quantities in equations 2.2 through 2.6 are idealized, ensemble averages. There is some variation within this class of model, for example the rate equation for h (entrainment relation) can alternatively be derived based on the turbulent kinetic energy budget (Federovich et al. [11]). But they are all based on the simplified $\overline{\theta}$ and $\overline{w'\theta'}$ profiles outlined above.

First (and higher) order models assume an entrainment layer (EL) of finite depth at the top of the ML, defined by two heights: the top of the ML (h_0) and the point where free atmospheric characteristics are resumed (h_1). The derivations are more complex and involve assumptions about the EL i.e.:

- $\Delta h = h_1 - h_0 = Constant$ (Betts 1974)
- $\Delta h = h_1 - h_0$ is related to the zero-order jump at h by two right angled triangles with opposite sides of lengths $h_1 - h$ and $h - h_0$ (Batchvarova and Gryning 1994)
- Δh or maximum overshoot distance $d \propto \frac{w^*}{N}$ where w^* is the convective vertical velocity scale to be defined in section 2.4.2 and $N = \sqrt{\frac{g}{\overline{\theta}}\frac{\partial\overline{\theta}}{\partial z}}$ is the Brunt-Vaisala frequency (Stull 1973)
- For $h_0 < z < h_1$ $\overline{\theta} = \overline{\theta}_{ML} + f(z,t)\Delta\theta$ where $f(z,t)$ is a dimensionless shape factor (Deardorff 1979, Federovich et al. 2004)

.

Although development of these models is beyond the scope of this thesis, they are mentioned to give context to the parametrizations considered.

2.3.2 Numerical Simulations

Numerical simulation of the convective boundary layer (CBL) is carried out by solving the Navier Stokes equations, simplified according to a suitable approximation, on a discrete grid. Types of simulations can be grouped according to the scales of motion they resolve. In direct numerical simulations (DNS) the full range of spatial and temporal turbulence are resolved from the size of the domain down to the smallest dissipative scales i.e. the Kolmagorov micro-scales. This requires a dense numerical grid and so can be computationally prohibitive.

In a large eddy simulation (LES) smaller scales are filtered out and parametrized by sub grid scale closure model. General circulation models (GCM) solve the Navier Stokes equations on a spherical grid and parametrize smaller scale processes including convection and cloud cover. LES has steadily, repeatedly been used to better understand the CBL since Deardorff (1972) applied this relatively new method for this purpose. Sullivan et al. (1998), Federovich et al. (2004) and Brooks and Fowler in (2012) used it to observe the structure and scaling behaviour of the EL.

2.4 Scales of the CBL and EL

2.4.1 Length Scale (h)

Deardorff (1972) demonstrated that dominant turbulent structures in penetrative convection scale with inversion height which was taken to be the height of minimum average vertical heat flux:z_f (Deardorff et al. 1980).

Since then, the definition of CBL height (h) has remained unchanged i.e. it is the height of the inversion or the vertical point, above the surface layer, of maximum change in tracer concentration or potential temperature (θ). There are alternatives. For example turbulence based definitions, such as the velocity variance and the distance over which velocity is correlated with itself, represent the current turbulent dynamics rather than the recent turbulence history as does h (Traumner et al. 2011).

2.4.2 Convective Velocity Scale (w^*)

Given an average surface vertical heat flux ($\overline{w'\theta'}_s$) a surface buoyancy flux can be defined as $\frac{g}{\theta}\overline{w'\theta'}_s$ from which the convective velocity scale is obtained by multiplying by the appropriate length scale. Since the result is in $\frac{m^3}{s^3}$ a cube root is applied

$$w^* = \left(\frac{gh}{\overline{\theta}}\overline{w'\theta'}_s\right)^{\frac{1}{3}} \tag{2.8}$$

.

Deardorff (1970) confirmed that this effectively scaled the local vertical turbulent velocity perturbations ($w^{'}$) in the CBL. Sorbjan's (1996) work supports this, even at the CBL top. $\frac{dh}{dt}$ and $w^{'}$ are driven by $\overline{w'\theta'}_s$ and inhibited by γ. The influence of γ on $w^{'}$ is indirectly accounted for via h in w^*.

2.4.3 Convective Time Scale (τ)

It logically follows that the time which a thermal travelling at velocity w^* takes to reach the top of the CBL, i.e. travel a distance h is

$$\tau = \frac{h}{\left(\frac{gh}{\overline{\theta}}\overline{w'\theta'}\right)^{\frac{1}{3}}} \tag{2.9}$$

.

This is also referred to as the convective overturn time scale. Sullivan et al. (1998) showed a linear relationship between h and time scaled by τ . An alternative is the Brunt-Vaisala frequency i.e. the time scale associated with the buoyant thermals overshooting and sinking (Federovich et al. [11]). The ratio of these two time-scales forms a parameter which characterizes this system (see Sorbjan1996 and Deardorff 1979).

2.4.4 Temperature Scales (θ^* and γ)

The CBL temperature fluctuations θ' are influenced by $\overline{w'\theta'}$ from both the surface and the CBL top. Deardorff (1970) showed that an effective scale based on the convective velocity scale is

$$\theta^* = \frac{\overline{w'\theta'}_s}{w^*} \tag{2.10}$$

Whereas Sorbjan (1996) showed that with proximity to the CBL top the effects of γ become more important.

2.4.5 Buoyancy Richardson Number (Ri)

The flux Richardson (R_f) number expresses the balance between mechanical and buoyant production of turbulent kinetic energy (TKE) and is obtained from the ratio of these two terms in the TKE budget equation (Stull 1988):

$$\frac{\partial \overline{e}}{\partial t} + \overline{U}_j \frac{\partial \overline{e}}{\partial x_j} = \delta_{i3} \frac{g}{\overline{\theta}} \left(\overline{u_i' \theta'} \right) - \overline{u_i' u_j'} \frac{\partial \overline{U}_i}{\partial x_j} - \frac{\partial \left(\overline{u_j' e'} \right)}{\partial x_j} - \frac{1}{\overline{\rho}} \frac{\partial \left(\overline{u_i' p'} \right)}{\partial x_i} - \epsilon \tag{2.11}$$

$$R_f = \frac{\frac{g}{\overline{\theta}} \left(\overline{w'\theta'} \right)}{\overline{u_i' u_j'} \frac{\partial \overline{U}_i}{\partial x_j}} \tag{2.12}$$

.

Assuming horizontal homogeneity and neglecting subsidence yields

$$R_f = \frac{\frac{g}{\overline{\theta}} \left(\overline{w'\theta'} \right)}{\overline{u'w'} \frac{\partial \overline{U}}{\partial z} + \overline{v'w'} \frac{\partial \overline{V}}{\partial z}} \tag{2.13}$$

.

Applying first order closure to the flux terms, i.e. assuming they are proportional to the vertical gradients, gives the gradient Richardson number (R_g)

$$R_g = \frac{\frac{g}{\overline{\theta}} \frac{\partial \overline{\theta}}{\partial z}}{\left(\frac{\partial \overline{U}}{\partial z}\right)^2 + \left(\frac{\partial \overline{V}}{\partial z}\right)^2} \tag{2.14}$$

,

which expresses the balance between shear and buoyancy production of TKE. However, in the EL buoyancy acts to suppress buoyant production of TKE. Applying a bulk approximation to the denominator, and expressing it in terms of scales yields a squared ratio of two time scales

$$R_g = \frac{\frac{g}{\overline{\theta}} \frac{\partial \overline{\theta}}{\partial z}}{\frac{U^{*2}}{L^2}} = N^2 \frac{L^2}{U^{*2}} \tag{2.15}$$

,

where U^* and L^* are appropriate velocity and length scales. Applying the bulk approximation to both the numerator and denominator yields the bulk Richardson number:

$$R_b = \frac{\frac{g}{\overline{\theta}} \Delta\theta L^*}{U^{*2}} \tag{2.16}$$

.

A natural choice of length and velocity scales for the CBL are h and w^* giving the convective or buoyancy Richardson number:

$$Ri = \frac{\frac{g}{\overline{\theta}} \Delta\theta h}{w^{*2}} \tag{2.17}$$

.

Ri can be arrived at by considering the principal forcings of the system, or from non-dimensionalizing the entrainment relation derived analytically (Tennekes 1973, Deardorff 1972). It is central to any study on CBL entrainment (Sullivan et al. 1998, Federovich et al. 2004, Traumner et al. 2011, Brooks and Fowler 2012).

2.4.6 Relationship of Entrainment Rate and Entrainment Layer Depth to Richardson Number

The relationship between scaled entrainment rate and the buoyancy Richardson number (Ri) is arrived at according the zero order bulk model through thermodynamic arguments, or by integration of the conservation of enthalpy or turbulent kinetic energy equations over the growing CBL. (Tennekes [24], Deardorff [8], Federovich et al. [11]).

$$\frac{w_e}{w^*} \propto Ri^{-a} \tag{2.18}$$

It has been verified in numerous laboratory and numerical studies (Deardorff et al. [9], Sullivan et al. [23], Federovich et al. [11], Brooks and Fowler [4]). But there is still some unresolved discussion as the the exact value of a. It seems there are two possible values, $-\frac{3}{2}$ and -1, the first of which Ellison and Turner (1959) suggested occurs at high stability when buoyant recoil of impinging thermals becomes more important than their convective overturning. Assume that an impinging thermal supplies kinetic energy per unit time and per unit area for entrainment, in terms of appropriate length and timescale L^* and t^* as follows

$$K \propto \frac{\overline{\rho} L^{*3} U^{*2}}{L^{*2} t^*} \tag{2.19}$$

,

and that the corresponding change in potential energy per unit time and area of the rising CBL is

$$\Delta P \propto g \Delta \rho h \frac{dh}{dt} \tag{2.20}$$

.

If L^* is the penetration depth of the thermals travelling at velocity w^* against a decelerating force $g\frac{\Delta\rho}{\overline{\rho}}$

$$L^* = \frac{w^{*2}\overline{\rho}}{\Delta\rho} \tag{2.21}$$

and the t^* is the response time of the inversion layer to a thermal of length h is

$$t^* = \sqrt{h\frac{\overline{\rho}}{g\Delta\rho}} \tag{2.22}$$

then assuming all of the kinetic energy (K) is transferred to the change in potential energy (ΔP) and using the CBL veloctiy, yields

$$\frac{\frac{dh}{dt}}{w^*} \propto \frac{w^{*2}\overline{\rho}}{g\Delta\rho h}\sqrt{\frac{\overline{\rho}w^*}{g\Delta\rho h}} \tag{2.23}$$

,
i.e.

$$\frac{w_e}{w^*} \propto Ri^{-\frac{3}{2}} \tag{2.24}$$

.
Adding further complexity to this discussion, Federovich et al. (2004) suggest that this power law relationship ($a = -\frac{3}{2}$) is arrived at through defining the θ jump accross the EL (see Figure 2.1).

A relationship of the scaled entrainment layer EL depth to Ri is arrived at by considering the deceleration of a thermal as it overshoots its neutral buoyancy level (Nelson et al. 1989). If the velocity of the thermal is assumed to be proportional to w^* and the decelerating force is due to the buoyancy difference, or θ jump, then the distance the thermal overshoots (d) can be approximated by

$$d \propto \frac{w^{*2}}{\frac{g}{\overline{\theta}_{ML}}\Delta\theta} \tag{2.25}$$

.
If the EL depth is proportional to the overshoot distance (d) then

$$\frac{\Delta h}{h} \propto \frac{w^{*2}}{\frac{g}{\overline{\theta}_{ML}} h \Delta\theta} = Ri^{-1} \tag{2.26}$$

Alternitavely, Boers 1989 integrated the internal (U), potential (P) and kinetic (K) energy over a hydrostatic atmosphere

$$U = \frac{c_v}{g} \int_0^{p_0} T dp \tag{2.27}$$

,

$$P = \frac{R}{c_v} U \tag{2.28}$$

and

$$K = \frac{1}{2} \int_0^{p_0} \frac{w^2}{g} dp \tag{2.29}$$

.

p_0 is the pressure the surface pressure, R and c_v are the gas constant and heat capacity of dry air at constant volume. T is temperature. Initially there is a flat infinitessimely thin inversion interface which is distorted by an impinging thermal. The resulting height difference is assumed sinusoidal and an average Δh is obtained by integrating over a wavelentgh. At this point, no entrainment is assumed to have occurred and all of the initial kinetic energy (K_i) has been transferred to the change in potential energy (ΔP).

$$K_i = P_f - P_i = \Delta P \tag{2.30}$$

Assuming a dry adiabatic atmosphere and that the vertical velocity in the layer below the inversion can be approximated by the convective velocity scale (w^*), the following expression is reached

$$\left(\frac{\Delta h}{h}\right)^2 \propto \frac{T_0 w^{*2}}{g \Delta\theta h} \tag{2.31}$$

The reference temperature, T_0, can be replaced by $\overline{\theta}_{ML}$ to give

$$\frac{\Delta h}{h} \propto Ri^{-\frac{1}{2}} \tag{2.32}$$

.

2.5 Approach to Research Questions

Similar to Sullivan et al. 1998, Federovich et al. 2004 and Brooks and Fowler 2012 I will model the dry shear free CBL and EL using LES, specifically the cloud resolving model System for Atmospheric Modelling (SAM) to be outlined in Chapter 3. I will use a slightly smaller domain than usuall (3.2x4.8 Km2 vs 5x5Km2) but will run a 10 case ensemble to obtain true ensemble averages and turbulent potential temperature perturbations (θ'). Grid spacing was influenced by Sullivan and Patton (2011) and the vertical grid within the EL is of higher resolution than the other comparable studies. Before addressing the questions stated in Section 2.1 I'll examine the modeled output to make sure it represents a realistic turbulent CBL in Chapter 3 section 2. I will verify that the averaged vertical profiles are as expected and coherent thermals are being produced. FFT energy density spectra will show if there is adequate scale separation between the most energy intense structures and the grid spacing, and that realistic, isotropic turbulence is being modelled. The runs will be initiallized with a constant $\overline{w'\theta'}_s$ acting a against a uniform γ. So here, the θ jump arises from the overshoot of the thermals, rather than being initially imposed as in Sullivan et al. (1998) and Brooks and Fowler (2012).

2.5.1 Q1: How do the distrubutions of local CBL height, and $w'\theta'$ within the EL, vary with $\overline{w'\theta'}_s$ and γ?

The EL can be thought of in terms of the distribution of indivual thermal heights, or local heights. Sullivan et al. (1998) measured local height by locating the vertical point of maximum θ gradient, and observed the effects of varying Ri on the resulting distributions. However this method is problematic when gradients in the upper profile exceed that at the inversion

(Brooks and Fowler 2012). Steyn et al. (1999) fitted an idealized curve to a lidar backscatter profile. This method produces a smooth curve based on the full original profile on which a mximum can easily be located. I will apply a multi-linear regression method outlined in Vieth (2011) to the local θ profile, representing the ML, EL and FA each with a separate line. From this fit, I will locate the ML top. I'll observe how the resulting distributions are effected by changes in $\overline{w'\theta'}_s$ and γ using histograms and verify that the resulting surface corresponds to the location of the termals in the EL, in Chapter 3 Section 3.

Sullivan et al. (1998) broke the turbulent vertical heat flux ($w^{'}\theta^{'}$) into four quadrants and used this combined with local flow visualizations to show how thermals impinge and draw down warm air from above. Mahrt and Paumier (1984) used 2 dimensional contour plots of local $w^{'}$ and $\theta^{'}$ measurements to analyse their joint distribubions. In his 1996 LES study Sorbjan showed that in the EL $\theta^{'}$ is strongly influenced by γ whereas $w^{'}$ is independent thereof. Influenced by these three studies, I will use 2 dimensional histograms at three levels within the EL to look at how the distrubutions of local $w^{'}$ and $\theta^{'}$ are effected by changes in γ and $\overline{w'\theta'}_s$. I will magnify the effects of γ, by applying the convective scales, θ^{*} and w^{*} in Chapter 3 section 4.

2.5.2 Q2: How can the EL limits be defined based on the $\overline{\theta}$ profile and what is the relationship of the resulting depth (Δh) to Ri?

Here I define the CBL height as the location of maximum vertical $\overline{\theta}$ gradient as in Figure 2.3. The lower and upper EL limits are then, the points at which $\frac{\partial\overline{\theta}}{\partial z}$ significantly exceeds zero and where it resumes γ. The lower limit requires choice of a threshold value which should be small, positive and less than γ. Since it is somewhat arbitrary I will compare results based on three different threshold values in Chapter 3 section 5. Federovich et al. (2004) and Brooks and Fowler (2012) defined the EL in terms of the vertical $\overline{w'\theta'}$ profiles as in Figure 2.3 but disagreed on the shape of the relationship of scaled EL depth to Ri (equation 2.1). As well as observing this relationship using the height defininitions based on the $\overline{\theta}$ profile, I will apply the definitions based on the $\overline{w'\theta'}$ profile for comparison with the Brooks and Fowler (2012) and Federovich et al. (2004) in Chapter 3 section 4.

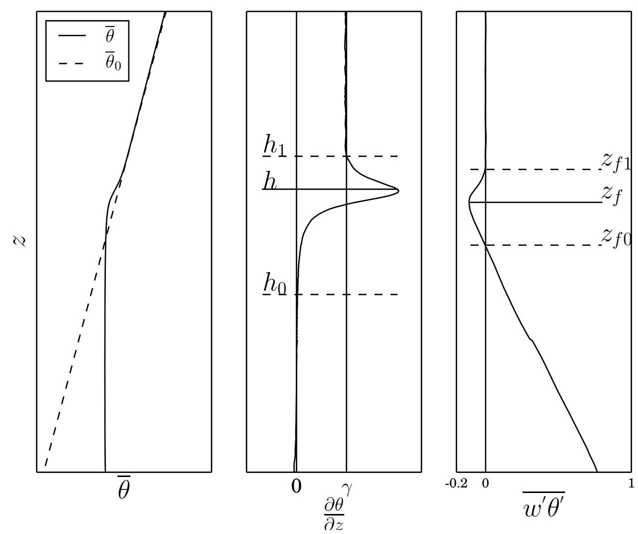

Figure 2.3: Height definitions based on the average vertical profiles. θ_0 is the inital potential temperature.

CBL Height	ML $\overline{\theta}$	θ Jump	Ri
h	$\overline{\theta}_{ML} = \frac{1}{h}\int_0^h \overline{\theta}(z)dz$	$\delta\theta = \overline{\theta}(h_1) - \overline{\theta}(h_0)$	$\mathrm{Ri}_\Delta = \frac{\frac{g}{\overline{\theta}_{ML}}\delta\theta h}{w^{*2}}$
		$\Delta\theta = \overline{\theta}_0(h) - \overline{\theta}_{ML}$	$\mathrm{Ri}_\delta = \frac{\frac{g}{\overline{\theta}_{ML}}\Delta\theta h}{w^{*2}}$

Table 2.1: Defintions based on the vertical $\overline{\theta}$ profile in Figure 2.3. To obtain those based on the $\overline{w'\theta'}$ profile, replace h_0, h and h_0 with z_{f0}, z_f and z_{f1}

2.5.3 Q3: How does defining the θ jump based on the vertical $\overline{\theta}$ accross the EL as in Figure 2.1 vs at the inversion (h) as in Figure 2.2, effect the entrainment relation, in particular a?

I will vary the definition of the θ jump and so Ri to see how this effects the resulting entrainment relation, as showin in table 2.1. In particular I wish to see the value of a so I'll plot in log coordinates. I will reproduce this plot using height definitions based on $\overline{w'\theta'}$ for comparison with the results of Federovich et al. (2004).

Bibliography

[1] E. Batchvarova and S.-E. Gryning. An applied model for the height of the daytime mixed layer and the entrainment zone. *Bundary-Layer Meteorology*, 71:311–323, 1994. → pages 12

[2] A. K. Betts. Reply to comment on the paper: "non-precipitating cumulous convection and its parametrization". *Quart. J. Roy. Meteor. Soc.*, 100:469 – 471, 1974. → pages 12

[3] R. Boers. A parametrization of the depth of the entrainment zone. *Journal of Applied Meteorology*, pages 107–111, 1989. → pages 4, 10, 19

[4] I. M. Brooks and A. M. Fowler. An evaluation of boundary-layer depth, inversion and entrainment parameters by large-eddy simulation. *Bundary-Layer Meteorology*, 142:245–263, 2012. → pages 2, 4, 7, 9, 10, 13, 17, 20, 21, 22

[5] T. D. Crum, R. B. Stull, and E. W. Eloranta. Coincident lidar and aircraft observations of entrainment into thermals and mixed layers. *Journal of Climate and Applied Meteorology*, 26:774–788, 1987. → pages 5, 6, 9

[6] J. W. Deardorff. Convective velocity and temperature scales for the unstable planetary boundary layer and for rayleigh convection. *Journal of the Atmospheric Sciences*, 27:1211 – 1213, 1970. → pages 2, 14, 15

[7] J. W. Deardorff. Numerical investigation of neutral and unstable planetary boundary layers. *Journal of the Atmospheric Sciences*, 29: 91 – 115, 1972. → pages 10, 13, 16

[8] J. W. Deardorff. Prediction of convective mixed-layer entrainment for realistic capping inversion structure. *Journal of the Atmospheric Sciences*, 36:424–436, 1979. → pages 4, 10, 12, 15, 17

[9] J. W. Deardorff, G. E. Willis, and B. J. Stockton. Laboratory studies of the entrainment zone of a convectively mixed layer. *J. Fluid Mech.*, 100:41–64, 1980. → pages 2, 4, 7, 9, 10, 13, 17

[10] T. H. Ellison and J. S. Turner. Turbulent entrainment in stratified flows. *Journal of Fluid Mechanics*, 6:423–448, 1959. → pages 17

[11] E. Federovich, R. Conzemus, and D. Mironov. Convective entrainmnent into a shear-free, linearly stratifies atmosphere: Bulk models reevaluated through large eddie simulation. *Journal of the Atmospheric Sciences*, 61:281 – 295, 2004. → pages 2, 4, 5, 7, 9, 10, 12, 13, 15, 16, 17, 18, 20, 21, 22, 23

[12] E. Fedorovich and R. Conzemius. *Large Eddy Simulation of Convective Entrainment in Linearly and Discretely Stratified Fluids.* Kluwer Academic Publishers, 1 edition, 2001. → pages 5

[13] J. R. Garcia and J. P. Mellado. The two-layer structure of the entrainment zone in the convective boundary layer. *Journal of the Atmospheric Sciences*, 2014. doi:10.1175/JAS-D-130148.1. → pages 2, 5, 8, 9, 10

[14] L. Mahrt and J. Paumier. Heat transport in the atmospheric boundary layer. *Journal of the Atmospheric Sciences*, 41:3061–3075, 1984. → pages 21

[15] E. Nelson, R. Stull, and E. Eloranta. A prognostic relationship for entrainment zone thickness. *Journal of Applied Meteorology*, 28: 885–901, 1989. → pages 2, 4, 6, 7, 10, 18

[16] H. Schmidt and U. Schumann. Coherent structure of the convective boundary layer derived from larg-eddy simulations. *J. Fluid. Mech.*, 200:511–562, 1989. → pages 5, 6, 7

[17] Z. Sorbjan. Effects caused by varying the strenth of the capping inversion based on a large eddie simulation of the shear free convective boundary layer. *Journal of the Atmospheric Sciences*, 53:2015 – 2023, 1996. → pages 2, 3, 7, 10, 14, 15, 21

[18] Z. Sorbjan. Similarity of scalar fields in the convective boundary layer. *Journal of the Atmospheric Sciences*, 56:2212 – 2221, 1999. → pages 7

[19] D. G. Steyn, M. Baldi, and R. M. Hoff. The detection of mixed layer depth and entrainment zone thickness from lidar backscatter profiles. *Journal of Atmospheric and Oceanic Technology*, 16:953–959, 1999. → pages 2, 9, 21

[20] R. Stull. Inversion rise model based on penetrative convection. *Journal of the Atmospheric Sciences*, 30:1092–1099, 1973. → pages 12

[21] R. Stull. *An Introduction to Boundary Layer Meteorology*. Kluwer Academic Publishers, 1 edition, 1988. ISBN 9027727686. → pages 1, 2, 5, 6, 15

[22] P. P. Sullivan and E. G. Patton. The effect of mesh resolution on convective boundary layer statistics and structures generated by large eddie simulation. *Journal of the Atmospheric Sciences*, 58:2395–2415, 2011. doi:10.1175/JAS-D-10-05010.1. → pages 20

[23] P. P. Sullivan, C.-H. Moeng, B. Stevens, D. H. Lenschow, and S. D. Mayor. Structure of the entrainment zone capping the convective atmospheric boundary layer. *Journal of the Atmospheric Sciences*, 55: 3042–3063, 1998. doi:10.1007/s10546-011-9668-3. → pages 2, 3, 5, 6, 7, 8, 9, 10, 13, 15, 16, 17, 20, 21

[24] H. Tennekes. A model for the dynamics of the inversion above a convective boundary layer. *Journal of the Atmospheric Sciences*, 30: 558–566, 1973. → pages 4, 11, 16, 17

[25] K. Traumner, C. Kottmeier, U. Corsmeier, and A. Wieser. Convective boundary-layer entrainment: Short review and progress using doppler lidar. *Bundary-Layer Meteorology*, 141:369–391, 2011. doi:10.1007/s10546-011-9657-6. → pages 2, 5, 6, 7, 8, 9, 10, 14, 16

[26] J. S. Turner. Turbulent entrainment: the development of the entrainment assumption and its application to geophysical flows. *J. Fluid Mech.*, 173:431–471, 1986. → pages 5

[27] E. Vieth. Fitting piecewise linear regression functions to biological responses. *Journal of Applied Physiology*, 67:390–396, 2011. → pages 21

Appendix A

Supporting Materials

A.1 Potential Temperature: θ

$$\theta = T\left(\frac{p_0}{p}\right)^{\frac{R_d}{c_p}} \tag{A.1}$$

p_0 and P are a reference pressure and pressure respectively.

$$\frac{c_p}{\theta}\frac{d\theta}{dt} = \frac{c_p}{T}\frac{dT}{dt} - \frac{R_d}{p}\frac{dp}{dt} \tag{A.2}$$

If changes in pressure are negligible compared to overall pressure, as in the case of that part atmosphere that extends from the surface to 2Km above it.

$$c_p\frac{d\theta}{\theta} = c_p\frac{dT}{T} - \frac{R_d}{p}\frac{dp}{p} \tag{A.3}$$

$$\frac{d\theta}{\theta} = \frac{dT}{T} \tag{A.4}$$

and if

$$\frac{d\theta}{dT} \approx 1 \tag{A.5}$$

$$\frac{d\theta}{\theta} = \frac{dT}{T} \tag{A.6}$$

A.2 Second Law of Thermodynamics

$$\frac{ds}{dt} \geq \frac{q}{T} \tag{A.7}$$

For a reversible process

$$\frac{ds}{dt} = \frac{q}{T} \tag{A.8}$$

Using the first law and the equation of state for an ideal gas

$$\frac{q}{T} = \frac{1}{T}\left(\frac{dh}{dt} - \alpha\frac{dp}{dt}\right) = \frac{c_p}{T}\frac{dT}{dt} - \frac{R_d}{p}\frac{dp}{dt} \tag{A.9}$$

so

$$\frac{ds}{dt} = \frac{q}{T} = \frac{c_p}{\theta}\frac{d\theta}{dt} \tag{A.10}$$

For a dry adiabatic atmmosphere

$$\frac{ds}{dt} = \frac{c_p}{\theta}\frac{d\theta}{dt} = 0 \tag{A.11}$$

A.3 Reynolds Decomposition and Simplification of Conservation of Enthalpy for a dry Atmosphere

$$\frac{\partial\theta}{\partial t} + u_i\frac{\partial\theta}{\partial x_i} = \nu_\theta\frac{\partial^2\theta}{\partial x_i^2} - \frac{1}{c_p}\frac{\partial Q^*}{\partial x_i} \tag{A.12}$$

ν and Q^* are the thermal diffusivity and net radiation respectively. If we ignore these two effects then (adiabatic?)

$$\frac{\partial\theta}{\partial t} + u_i\frac{\partial\theta}{\partial x_i} = 0 \tag{A.13}$$

$$\theta = \overline{\theta} + \theta^{'}, \theta = \overline{u_i} + u_i^{'} \tag{A.14}$$

$$\frac{\partial\overline{\theta}}{\partial t} + \frac{\partial\theta^{'}}{\partial t} + \overline{u_i}\frac{\partial\overline{\theta}}{\partial x_i} + u_i^{'}\frac{\partial\overline{\theta}}{\partial x_i} + \overline{u_i}\frac{\partial\theta^{'}}{\partial x_i} + u_i^{'}\frac{\partial\theta^{'}}{\partial x_i} = 0 \tag{A.15}$$

Averaging and getting rid of average variances and their linear products

$$\frac{\partial\overline{\theta}}{\partial t} + \overline{u_i}\frac{\partial\overline{\theta}}{\partial x_i} + u_i^{'}\frac{\partial\theta^{'}}{\partial x_i} = 0 \tag{A.16}$$

Ignoring mean winds

$$\frac{\partial\overline{\theta}}{\partial t} + u_i^{'}\frac{\partial\theta^{'}}{\partial x_i} = 0 \tag{A.17}$$

using flux form

$$\frac{\partial\overline{\theta}}{\partial t} + \frac{\partial(u_i^{'}\theta^{'})}{\partial x_i} - \theta^{'}\frac{\partial u_i^{'}}{\partial x_i} = 0 \tag{A.18}$$

under the bousinesq assumption $\Delta \dot{u}_i = 0$

$$\frac{\partial\overline{\theta}}{\partial t} = -\frac{\partial(u_i^{'}\theta^{'})}{\partial z} \tag{A.19}$$

ignoring horizontal fluxes

$$\frac{\partial\overline{\theta}}{\partial t} = -\frac{\partial(w^{'}\theta^{'})}{\partial z} \tag{A.20}$$

A.4 Reynolds averaged Turbulence Kinetic Energy Equation

$$\frac{\partial\overline{e}}{\partial t} + \overline{U}_j\frac{\partial\overline{e}}{\partial x_j} = \delta_{i3}\frac{g}{\overline{\theta}}\left(\overline{u_i^{'}\theta^{'}}\right) - \overline{u_i^{'}u_j^{'}}\frac{\partial\overline{U}_i}{\partial x_j} - \frac{\partial\left(\overline{u_j^{'}e^{'}}\right)}{\partial x_j} - \frac{1}{\overline{\rho}}\frac{\partial\left(\overline{u_i^{'}p^{'}}\right)}{\partial x_i} - \epsilon \tag{A.21}$$

e is turbulence kinetic energy (TKE). p is pressure. ρ is density. ϵ is viscous dissipation.